Supplementary Information for: "Dispersal of fungal spores on a cooperatively generated wind"

Marcus Roper*,[1,2] Agnese Seminara,[3] M. M. Bandi,[3]
Ann Cobb,[4] Helene R. Dillard,[4] and Anne Pringle[5]

[1]*Dept. of Mathematics and Lawrence Berkeley National Lab, University of California, Berkeley, CA 94720*

[2]*Mathematics Institute, University of Warwick, Coventry, CV4 7AL, UK*

[3]*School of Engineering and Applied Sciences, Harvard University, Cambridge, MA 02138*

[4]*Dept. of Plant Pathology and Plant-Microbe Biology, Cornell University and New York State Agricultural Experiment Station, Geneva, NY 14456*

[5]*Dept. of Organismic and Evolutionary Biology, Harvard University, Cambridge, MA 02138*

Abstract

This document includes the following Supplementary Information for the paper: "Dispersal of fungal spores on a cooperatively generated wind"

I Design and validation of a numerical algorithm for simulating spore trajectories

II Spore flux data from real fungal fruit bodies.

III Direct measurement of the speed of spore launch in *Sclerotinia sclerotiorum*.

IV Derivation of an analytic expression for the range of collectively ejected spores.

V Numerical verification of the asymptotic analysis of the entrainment of air by a rising sheet of spores.

VI Statistics of spore ejection times in *Ascobolus* cf. *furfuraceus*.

* To whom correspondence should be addressed. E-mail: mroper@math.berkeley.edu

I. DIRECT NUMERICAL SIMULATIONS OF THE SPORE LADEN JET

Simulations of the two-way interaction between fluid motion and dispersed particles have been carried out extensively in the past [1]. Spore jets are in the limit discussed in [2] where the spore mass loading is appreciable ($\sim 10\%$) but the volume loading is considerably less than 1 ($\sim 10^{-4}$) so that excluded volume effects can be neglected. Spores are approximated by rigid spheres of radius r, mass m_s and density ρ_s. Their response timescale $\tau = 2r^2\rho_s/(9\nu\rho_a) \approx$ (1 to 6) ms (where ρ_a and ν are density and kinematic viscosity of air) is comparable with the shortest timescale of the jet, which is defined as the diameter of the apothecium divided by the maximum velocity of the centerline (2 to 11 ms). Therefore, spore trajectories are not ballistic, but follow the streamlines of the air flow with a delay of order τ. The Reynolds number based on spore velocity and diameter is larger than 1 at injection. In few ms spores decelerate to velocities smaller than 1 $\mathrm{m{\cdot}s^{-1}}$ so that their Reynolds number rapidly decreases below 1 and non-linear corrections to the drag force are negligible. In this regime spores are independent Stokes particles:

$$\frac{d\mathbf{x}_i}{dt} = \mathbf{u}_i \tag{S1}$$

$$\frac{d\mathbf{u}_i}{dt} = -\frac{\mathbf{u}_i - \mathbf{u}(\mathbf{x}_i)}{\tau} + \mathbf{g} \tag{S2}$$

where $\mathbf{u}_i$ and $\mathbf{x}_i$ are velocity and position of the i-th spore and $\mathbf{u}(\mathbf{x}_i)$ is the air velocity interpolated from the gridpoints to the particle position.

We expect the neglect of finite Reynolds number effects to alter the dynamics of air mobilization at the base of the jet, where the spore Reynolds number may exceed 1. We quantify these errors in Section IV.

In contrast to the particle Reynolds number, the Reynolds number based on the velocity and diameter of the jet is considerably larger than 1 (up to 250), so that the Stokes approximation for the flow fails and numerical simulations of the full Navier-Stokes equations are required to model the acceleration of air by spores. In order to simulate the flow generated by the cloud of spores we couple the motion of spores and surrounding fluid with two-way interactions to be discussed in detail in Section I C. To solve for the flow of air we treat spores as point forces with intensity equal the instantaneous drag force experienced by the

Table S1: Values of the parameters used in the simulations. Top, from left: type of ejection; spore launch speed v_s; diameter of the apothecium D; spore Reynolds number at injection Re_s; jet Reynolds number Re. Bottom, from left: air kinematic viscosity ν; spore density ρ_s; spore radius r; velocity of propagation of the puffing wave v_w, see Section II (duration of the puff $t_{\text{puff}} = D/v_w$); density of asci on the hymenium σ, reported experimental values range from about 400 mm^{-2} (see Section II) to about 1200 (see [3]). The effective number of spores is $n = \sigma\pi D^2/4$ (the 8 spores inside every ascus are launched together and the effective spore radius is $2r$).

	ejection	v_s $[\frac{m}{s}]$	D $[mm]$	Re_s	Re
R2	random	2	1.1 2.3 3.4 4.5 5.6	2.6	45 90 130 150 180
R4	random	4	0.6 1.1 1.7 2.2 2.8 3.3 3.9 4.5 5.1	5.3	30 50 60 80 100 110 120 130 140
C2	coordinated	2	3.4	2.6	250
C4	coordinated	4	3.4	5.3	180

$\nu[m^2/s]$	$\rho_s[g/cm^3]$	r $[\mu m]$	$v_w[\frac{m}{s}]$	σ $[mm^{-2}]$
1.5×10^{-5}	1	10	0.015	10^3

spore. The system of Eulerian equations to be integrated numerically is:

$$\boldsymbol{\nabla} \cdot \mathbf{u} = 0 \tag{S3}$$

$$\partial_t \mathbf{u} + \mathbf{u} \cdot \boldsymbol{\nabla}\mathbf{u} = \nu\Delta\mathbf{u} - \frac{1}{\rho_a}\boldsymbol{\nabla}p + \frac{1}{\rho_a}\sum_{i=1}^{n} m_s \frac{\mathbf{u}_i - \mathbf{u}(\mathbf{x_i})}{\tau}\delta(\mathbf{x} - \mathbf{x}_i) \tag{S4}$$

$$\tag{S5}$$

where $\mathbf{u}$ is the air velocity field and ν and p are viscosity and pressure. We perform four series of simulations: R2 and R4, corresponding to random uniformly ejected spores, and C2 and C4, corresponding to spatially coordinated sequence of spore ejections, covering the parameter ranges listed in table S1. In the following subsections we describe the physical parameters that are input into our simulations and validate the numerical model both by comparing with exactly solvable flow fields and by testing for sensitivity to the mesh size and size of the computational domain.

A. Algorithms

The Lagrangian trajectories of the spores are integrated in time using a second order Runge-Kutta algorithm. Spores are initially distributed randomly with uniform probability on a circular apothecium of diameter D at $z = z_0$. Over a time interval $t_{\rm puff} = D/v_w$ all the spores are released with initial vertical velocity v_s. To dissect the effect of varying the timing, positions and speeds of ejected spores upon the dynamics of air entrainment by the spore jet we perform four series of simulations. Spores are ejected randomly for series R2 and R4, whereas in simulations C2, C4 puffing starts from a point on the rim of the apothecium and propagates across the apothecium as a circular wave with constant velocity v_w. Series R2 and R4 examine the hydrodynamics of spore/air interaction and explore how the range of the spores changes as a function of the size of the apothecium. Simulations C2 and C4 investigate the range modification due to delayed launch time of a possible cheater. The full Navier-Stokes equations in potential vector form [4] are integrated in three dimensions with a pseudospectral method on a 256^3 cubic lattice with second-order Runge-Kutta scheme for time marching, periodic boundary conditions and 8/9 de-aliasing. The initial condition for the three components of the air velocity field is zero. We ensure that the computational domain is large enough so that for the timescale of the computation the boundary conditions do not affect the results.

Simulations C2, C4 are designed to determine whether the range of a spore can be increased by delaying the launch time of a time lag T', imposing additional constraints upon the accuracy of integration of individual spore trajectories. Besides the trajectory of all the collaborators we add the evolution of a hypothetical cheater and repeat its integration by changing its initial position and its launch time. The cheater is assumed to be passive; specifically we neglect any modification of the fluid flow caused by perturbation to the trajectory of a single spore. Tests have been performed in order to check that a single spore does not modify appreciably any other trajectory. The timescale T' spans from 0 to $t_{\rm puff}$ in 200 steps (where $t_{\rm puff} = D/v_w$ is the duration of the puff). This choice insures that the range differences between cheating trajectories with different launch time are not artifacts of the algorithm (see section I B).

B. Interpolation and extrapolation

Particles are not restricted to lie on the grid points, hence a function S is needed to interpolate the fluid velocity at arbitrary spore positions from the nearby grid points: $\mathbf{u}(\mathbf{x}_i) = \sum_g S(\mathbf{x}_g, \mathbf{x}_i)\mathbf{u}_g$, where $\mathbf{u}_g$ is the velocity at the location $\mathbf{x}_g$ of the grid points and S is such that $\sum_g S(\mathbf{x}_g, \mathbf{x}_i) = 1$. Conversely, the point force computed at spore center must be extrapolated to the surrounding grid points, so that a backward interpolation function S^* is needed. The discrete representation of the δ-functions $\delta(\mathbf{x} - \mathbf{x}_i)$ is $S^*(\mathbf{x}_g, \mathbf{x}_i)/V_g$ where V_g is the volume of the grid cell. Conservation of total energy requires that S be the same as S^* [5]. Clearly, the details of the flow at scales comparable with the grid cell depend on the form of this function, as thoroughly discussed in [2]. These details do not influence the large scale structures that determine the range of the jet when spores are ejected randomly (series R2 and R4). However, they may affect simulations C2, C4, in which the trajectories of spores started from slightly different initial conditions are compared, so that the fine scale details of the flow may become important. In order to avoid any possible artifact we design simulations C2, C4 such that only differences in the flow at scales larger than the grid cell matter. Namely, we compare different replicas of the cheating spore whose trajectories are always farther apart than 1 grid cell. In Fig. S1 (left panel) we show the gain in the range of a cheating spore in two runs C2 with identical parameters (see Tab. S1) and different function S (linear and second order Lagrangian polynomial). In the right panel we show the corresponding energy spectra. Comparison of the results proves consistency of the algorithm. All the results shown in the main body of the paper have been obtained with the second order polynomial scheme.

C. Point force scheme and boundary conditions

In order to faithfully reproduce the effect of a spore travelling in air one should solve the equations of motion with no-slip boundary conditions at the spore surface. This level of description is impractical when dealing with tens of thousands of particles. For relatively dilute suspensions there have been a number of investigations treating the particles as point masses (see e.g. [6]). The pointwise approximation of the hydrodynamic interactions represents properly the velocity field far from the particle. Fig. S2 shows the velocity field

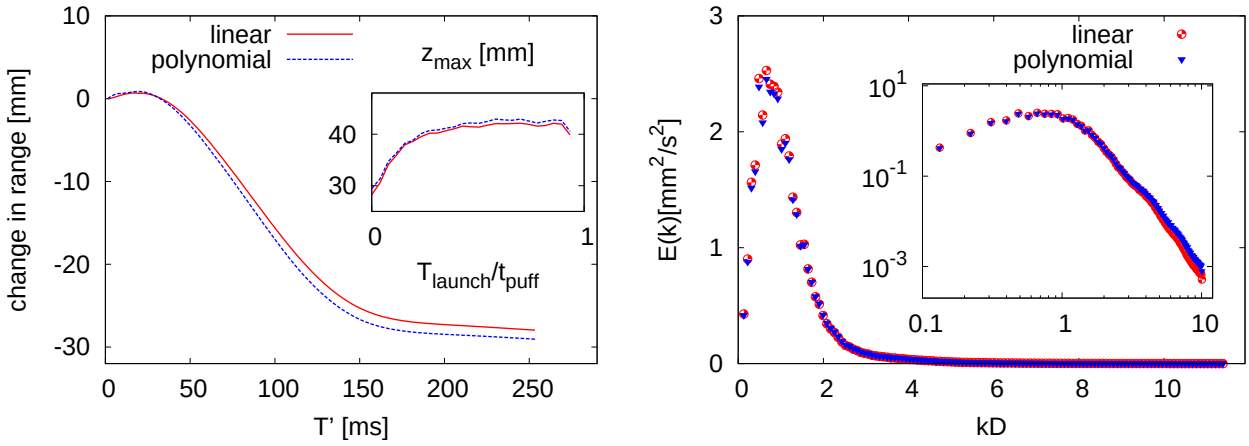

Figure S1: Left panel: simulation C2, range difference between a collaborating spore and a cheater starting with the same initial position and launch time delayed by T' (average over all initial positions). Parameters of the simulation are shown in Table S1. Red solid (blue dotted) line: results obtained with first (second) order Lagrange polynomial for the interpolation/extrapolation schemes. Inset: maximum height achieved by the collaborating spores as a function of their launch time. The comparison shows robustness of the result with respect to the algorithm for extrapolation of the point forces and interpolation of the fluid velocities at particle positions. Right panel: corresponding energy spectra (symbols as shown in the figure), at time $t = 100\,ms$. $E_k = 1/2 \int_{S_k} |\hat{\mathbf{u}}(\mathbf{k})|^2 dS$, where $\hat{\mathbf{u}}$ is the 3D Fourier transform of the velocity field, $\mathbf{k}$ is the wavenumber vector, S_k is the shell of wavenumbers such that $|\mathbf{k}| = k$ and $dS = k^2 d\Omega$ is the element of surface on the shell, $d\Omega$ is the elementary solid angle. The peak in the energy spectrum is at $k \sim 1/D$, showing that the correlation length of the flow is the diameter of the apothecium. The details of the energy spectrum at small wavelength depend weakly on the interpolation/extrapolation method.

produced by one isolated spore, moving at constant velocity of 0.5 m·s^{-1}. The simulation is done in the comoving frame where the particle is standing still in the center of the domain. The flow field converges to the Oseen solution at all distances except at the very grid cell where the particle is standing. We tune our simulation in order to resolve properly the interparticle distance (at our volume fractions, the interparticle distance is always larger than about 0.7 mm, and the grid scale is about 0.2 mm).

Note that this test also shows that the boundary conditions do not influence the solution until the Oseen wake extends to the bottom edge of the domain. This timescale can be

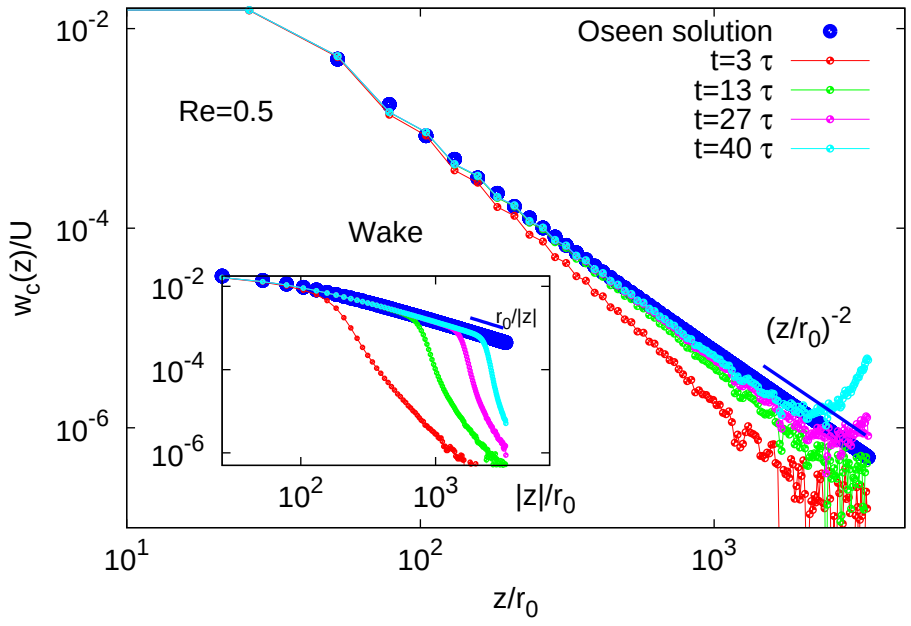

Figure S2: Vertical component of the fluid velocity produced by a single spore of radius $r_0 = 10\,\mu m$ moving at constant velocity $U = 0.5\,\mathrm{m{\cdot}s^{-1}}$ along the z axis. Different colors correspond to different timepoints. The particle is located at the origin in the comoving frame. The velocity converges to the Oseen solution, computed at the grid points, everywhere except in the grid cell containing the spore. Boundary conditions artifacts come into play only after the wake of the Oseen solution reaches the edge. This occurs in a timescale $\sim L/w \sim 40\,\tau$ where L is the size of the box and w is the velocity of the spore. No such estimate is possible for the unsteady state, for which additional tests have been performed (see Fig. S3).

estimated for this simple case as the size of the domain divided by the constant velocity of the spore, and turns out to be consistent with the results. There is no such simple estimate for the case of multiple spores in a non-steady state. In order to make sure that there are no boundary-condition artifacts we simply compare the results of simulation C2 with two different sizes of the domain (see Fig. S3). The results shown in the main body of the paper are obtained with a vertical box size of about 4/3 of the height of the jet (in between the two cases shown in Fig. S3). The horizontal box size has been reduced in simulation C2, C4 in order to adequately resolve the thickness of the sheet (see Section V).

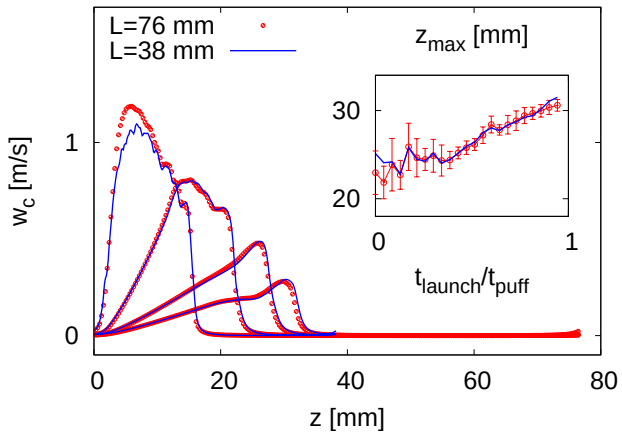

Figure S3: Main figure: Vertical velocity along the centerline of the jet, at $t = 30$, 50, 70, 90 ms, for simulation C2 (same parameters as in the main text, except for $D = 1.1$ mm) obtained with two different sizes L of the computational domain: $L = 76$ mm (red circles) and $L = 38$ mm (blue solid line). Inset: range of the collaborating spores as a function of the launch time, averaged over time lags of about 4 ms, same symbol as in the main frame. Fate dispersion due to different Lagrangian histories (represented by the errorbars) is larger than the small artifact due to periodic boundary conditions.

II. SPORE FLUX MEASUREMENTS FROM REAL APOTHECIA

As described in the Materials and Methods section (main text) we infer the spore flux from real apothecia by measuring independently the dependence of the number of ejected spores, and the puff duration, upon the diameter of the apothecium (Fig. S4).

III. DIRECT MEASUREMENT OF SPORE EJECTION VELOCITIES IN *SCLEROTINIA SCLEROTIORUM*

As described in the Materials and Methods section (main text) we estimate the ejection velocities for *Sclerotinia sclerotiorum* directly from the same high speed movies used to measure the speeds of spores in the jet. In the basal region of the jet, spores travel 3 to 8 pixels during a single frame, so that they appear as streaks (Fig S5a, and Supporting Movie 2). Although PIV is not possible, because of the difficulty of locating spores in consecutive frames, we can estimate the spore launch speed by dividing the length of the streaks by the

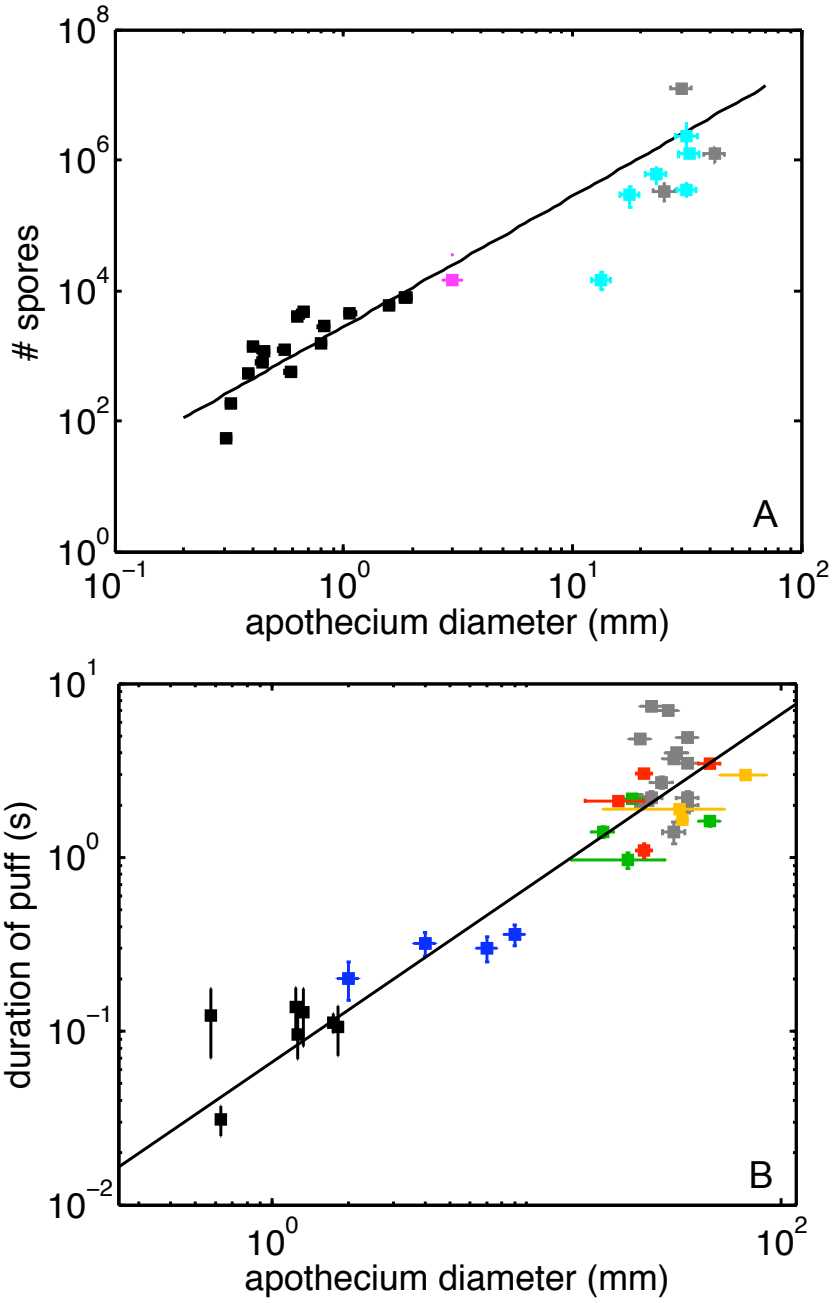

Figure S4: Measurements of duration of puff and number of spores ejected during puff support a conserved mechanism for synchronizing ejections from different asci and a constant spore flux, independent of species and equal among different individual fruit bodies. (A) Number of ejected spores, N, increases with the square of the fruit body diameter, D. Black line gives the best fit: $N = 3500$ spores/mm^2 $\times \left(\frac{1}{4}\pi D^2\right)$. (B) Duration of the puff, t_{puff} increases linearly with the fruit body diameter. Black line gives the best fit: $t_{\text{puff}} = 66.5\text{ms/mm} \times D$. Different colors correspond to different genera: *Ascobolus* (black), *Sclerotinia* (blue), *Geopyxis* (green), *Caloscypha* (red), *Helvella* (grey), *Sarcosphaera* (orange), *Cheilymona* (magenta), *Peziza* (cyan).

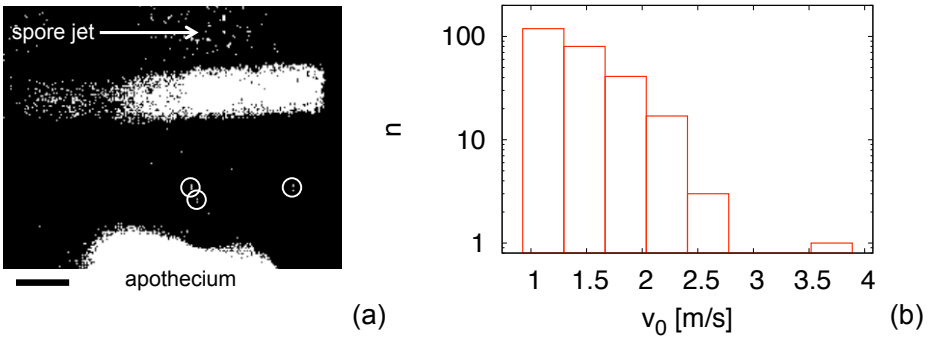

Figure S5: (a) Frame from high speed movie of spore launch in *Sclerotinia sclerotiorum*. Spores appear as streaks (circled) close to the apothecium, before decelerating to form a coherent jet (top half of the image). The horizontal band in the middle of the image is light scattered from the rim of the petri dish containing the fruit body. Scale bar: 2 mm. (b) Histogram of spore ejection velocities measured from spore streaks. At a distance of $\sim$ 1 mm from the fruit body, spores have velocity (2.6 ± 0.4)m/s

exposure time. We are able to locate streaks between 1 and 2 mm from the fruit body, by which time spores are moving between 1 and 3 m/s (Fig. S5b shows the histogram based on the estimated velocities of 262 spores). Because few spores will travel perfectly parallel to the laser sheet, some streaks are foreshortened when the spore leaves the plane of illumination. For this reason, we expect the most probable velocity to be the highest recorded value i.e. (ignoring the largest velocity, which was recorded for 1 spore) (2.6 ± 0.4) m$\cdot$s^{-1}. However, spores steeply decelerate over the first mm after leaving the fruit body. A single spore of *S. sclerotiorum* has typical dimensions of 10 to 14 μm $\times$ 4 to 5 μm [7], so spores decelerate by $\approx$ 5.8 m$\cdot$s^{-1} for every mm that they travel. Accordingly, we take the initial speed of spores to be $v_s \approx 8.4$ m$\cdot$s^{-1}, which agrees quite well with previously measured speeds of ejection for the discomycete *Ascobolus immersus* [8]. For this speed of ejection, and spore size, the total range of a single ejected spore is then only 1.4 mm, which is a factor of 20 less than the measured length of spore jets formed when spore ejection is synchronized over the apothecium.

IV. AN ANALYTIC EXPRESSION FOR THE RANGE OF COLLECTIVELY LAUNCHED SPORES

Here we develop an expression for the variation of the cross-section averaged velocity of the jet ($u_j(z)$) with height. We separately analyze the dynamics of the jet in two regions, according to whether $u_j(z)$ is increasing or decreasing with height (see Fig S7A). A similar hydrodynamic analysis allows us to compute the velocity profile for a sheet of upward moving spores and thereby to prove that a spatial organization can target cooperative benefits to cooperating spores (main text, Methods and Materials).

A. Acceleration region

Within the lowest part of the jet, spores, with speed $u_s(z)$ decelerate into almost still air. The surrounding fluid in turn is then accelerated, until spores and fluid move at the same speed, U. Momentum is therefore donated from spores to a region of entrained fluid, not much larger in size than the apothecium. Balancing this momentum against the momentum input by the ejected spores gives:

$$m_s q_s u_s + \rho u_j^2 = m_s q_s v_s \ . \tag{S6}$$

The air gains momentum proportional to the fluid drag on the spores, so that if the average concentration of spores is $n(z)$, and the Stokes' drag coefficient for a single spore is ζ, then:

$$\frac{d}{dz}\rho u_j^2 = -n\zeta(u_j - u_s) \ . \tag{S7}$$

Since spores do not escape from the sides of the jet, the number flux of spores must be conserved with height, giving: $nu_s = q_s$. We use this expression to substitute for n, and Eq.(S6) to substitute for u_s in Eq.(S7). We also scale all speeds by the ejection speed v_s and all lengths by the range of a spore in still air: $L_s = m_s v_s/\zeta$ [9], to obtain:

$$2\left(M - u_j^2\right)\frac{u_j}{M}\frac{du_j}{dz} = -u_j^2 + M\left(u_j - 1\right) \ , \tag{S8}$$

in which a new dimensionless parameter $M = m_s q_s/\rho v_s \equiv m_s n(z=0)/\rho$ appears, representing the mass density of spores at the foot of the jet. Eq.(S8) may be integrated by separation of variables to obtain a closed form expression for the dependence of jet speed

on height within the lowest part of the jet:

$$\frac{2}{M}\left(\frac{u_j^2}{2} - u_j M + \frac{M^2(1+M)}{S}\log\left[\frac{(S+2u_j+M)(S-M)}{(S-2u_j-M)(S+M)}\right] + \frac{M^2}{2}\log\left[\frac{M(1-u_j)-u_j^2}{M}\right]\right) = z\,, \tag{S9}$$

where we have defined a new variable $S = \sqrt{M^2+4M}$. This equation describes evolution of the average jet speed from $u_j = 0$ at $z = 0$, up to the point where spores and air move with identical velocity $u_s = u_j = U = \frac{1}{2}(S-M)$. Note however that the equation predicts an unphysical divergence in z as $u_j \to U$: put simply, the equation implies that spores travel infinitely far before air and spores travel at the same speed. However, the singularity is only logarithmic:

$$z \sim \left(M - \frac{2M(1+M)}{S}\right)\log(U-u_j)\,, \tag{S10}$$

so that any of the non-modelled corrections to this profile, either from gravity or from viscous stresses around the periphery of the jet, will eventually be sufficient to decelerate spores to the speed of the surrounding fluid. Accordingly, we use the predicted jet profile (S9) only until u_j reaches some fixed fraction, very close to 1, of the final velocity U. To compare with our simulations, we have taken $0 < u_j < 0.999U$, but because the divergence of z is only logarithmic, the jet profile depends only very weakly on the value that we choose for this cutoff speed.

Within the acceleration region the Reynolds number of individual spores may exceed 1. This may lead to quantitative errors in the DNS predictions for the jet dynamics. To demonstrate that these errors are small, we add finite Reynolds number effects directly into our asymptotic model for the dynamics of the acceleration region. The mass and momentum conservation laws (in particular, Eq. S6) are unaffected. However, the drag law for single spores must be modified. Since spores are much denser than the surrounding fluid, unsteady flow effects are not important [17] and we can introduce a simple Reynolds number-controlled drag correction

$$\frac{d}{dz}\rho u_j^2 = -n\zeta(u_j - u_s)f(\mathcal{R}e)\,. \tag{S11}$$

Although, in general it is not possible to write down an analytic solution to the resulting set equations, they may be integrated numerically to obtain the dependence of the jet velocity upon height within the acceleration region. We compared the solutions using the Stokes drag law S7 with finite Reynolds number approximations to the spore drag S11, using

$v_s(m/s)$	Stokes drag	White (Eq. S12)	Pruppacher and Steinberger (Eq. S13)
1	3.5	3.3	3.4
2	6.6	6.1	6.2
4	12.4	10.7	10.9
10	28.1	21.6	22.0

Table S2: Length of acceleration region in mm (here defined as the region in which u_j increases from 0 to $0.999U$, using different drag laws and initial spore velocities, v_s.

the empirical finite Reynolds number drag corrections of White [10]:

$$f(\mathcal{R}e) = 1 + \frac{\mathcal{R}e}{6\pi}\left(\frac{3}{1+\sqrt{2\mathcal{R}e}} + 0.2\right) \ , \tag{S12}$$

and of Pruppacher and Steinberger [11]:

$$f(\mathcal{R}e) = \begin{cases} 1 + 0.102(2\mathcal{R}e)^{0.96} & \text{for} \quad \mathcal{R}e < 1 \\ 1 + 0.115(2\mathcal{R}e)^{0.80} & \text{for} \quad \mathcal{R}e > 1 \end{cases} \tag{S13}$$

In particular, the velocity of the spores and air at the end of the basal region is given only by conservation of spore and air momentum and of spore mass, and is therefore independent of the process whereby momentum is transferred from spores to the air (Fig. S6). However, the drag law for the spores sets the distance over which this momentum transfer occurs, and thus ultimately determines the length of the acceleration region. In fact we found that finite inertial effects quantitatively changed the length of the acceleration region by up to 6 mm for the fastest ejected spores (Table S2). In real terms this means that our simulations may mis-locate the boundary between accelerating and decelerating regions of the jet by up to 6 mm but provide a quantitatively correct picture of the jet dynamics above this height.

B. Deceleration region

In the upper region of the jet spores and air move together, but are decelerated by gravity and by viscous stresses. Since spores approximately follow the streamlines of the incompressible air flow, we assume that the density of spores is uniform within the jet. Then balancing gravity and viscous stresses against inertia on a slice of the jet yields Eq.(1), which describes the velocity within the jet as it decelerates from $u_j = U$ at $z = z_I$ to $u_j = 0$. If

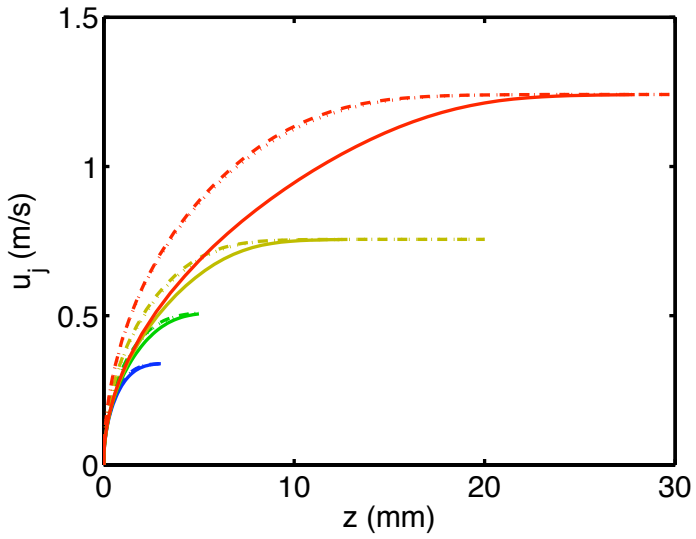

Figure S6: Predicted air speed in the acceleration region, including and excluding the finite Reynolds number of spores. Solid curves are the predictions using the Stokes drag relation, and broken curves using empirical relations for the drag upon a spore from White (dashed) and Pruppacher and Steinberger (dotted). Flow profiles are colored according to the initial speed of spores: v_s = 1 (blue), 2 (green), 4 (yellow), 10 m·s^{-1} (red). Although accounting for finite $\mathcal{R}e$ effects slightly changes the distance over which the air speed is accelerated to U, the value of U is unaffected by the form of the drag law.

we completely neglect the viscous stresses upon the jet, then this equation can be simply integrated by separation of variables:

$$z - z_I = \frac{\rho(U^2 - u_j^2)}{2(\rho + \rho_s)g} \tag{S14}$$

Eq.(S14) significantly over-predicts the range of the jet. In order to better model the jet profile, it is necessary to include the contribution of viscous stresses. Since there is little relative motion between spores and surrounding air (Fig 2B), these stresses originate from regions of high fluid shear between the upward moving spore carrying air, and surrounding still air. Since the Reynolds number of the jet is large ($Re \equiv Ua/\nu > 100$), we expect this shear to be restricted to thin boundary layers around the circumference of the jet, and this is confirmed when we plot the shear gradients from our DNS (Fig S7B). Accordingly, we can use the self-similar structure of these viscous boundary layers [12] to produce analytic expressions

for the total drag on the jet. We calculate the viscous contribution to the deceleration of the spore jet by a perturbative expansion for the jet speed $u_j = u_j^{(0)} + u_j^{(1)} + \ldots$ and area $A_j = A_j^{(0)} + A_j^{(1)} + \ldots$. $u_j^{(0)}$ is given by inviscid jet profile of Eq.(S14), while $A_j^{(0)}$ can be obtained from mass conservation: $A_j^{(0)} = \pi a^2 U/u_j^{(0)} \approx \pi a^2$, over the region of the jet in which the boundary layer contribution is strongest. $u_j^{(1)}$ and $A_j^{(1)}$ together satisfy the linearized form of Eq.(1):

$$(\rho + \rho_s) u_j^{(0)} A_j^{(0)} \frac{du_j^{(1)}}{dz} = F_{\text{visc}}[u_j^{(0)}] - \rho_s g A_j^{(1)} \tag{S15}$$

and the conservation of mass condition: $u_j^{(1)} A_j^{(0)} = -u_j^{(0)} A_j^{(1)}$.

We assume that the viscous boundary layer is much thinner than the radius of the spore jet and define a local coordinate y and velocity field component v, across the boundary layer. Additionally, we assume that the deceleration of the jet is much smaller than gravitation deceleration, so that we can make a Boussinesq approximation within the boundary layer (i.e. neglect the effect of spores upon the inertia of the jet, but retain their contribution to the gravity force [13]). Under these assumptions, the leading order velocity is given by the solution of the two dimensional boundary layer equations [12]:

$$u\frac{\partial u}{\partial z} + v\frac{\partial u}{\partial y} = -u_j^{(0)} \frac{du_j^{(0)}}{dz}\chi + \nu \frac{\partial^2 u}{\partial y^2} , \tag{S16}$$

$$\frac{\partial u}{\partial z} + \frac{\partial u}{\partial y} = 0 . \tag{S17}$$

with the first term on the right hand side representing the weight of the spore laden air, and the indicator function χ set equal to 1 within the jet, and 0 outside of the jet. It is usual to collect these equations into a single equation of higher order, by defining a streamfunction ψ so that:

$$u = \frac{\partial \psi}{\partial y} \quad \text{and} \quad v = -\frac{\partial \psi}{\partial z} , \tag{S18}$$

so that Eq.(S17) is automatically satisfied [14], and Eq.(S16) may be rewritten as:

$$\frac{\partial \psi}{\partial y}\frac{\partial^2 \psi}{\partial y \partial z} - \frac{\partial \psi}{\partial z}\frac{\partial^2 \psi}{\partial y^2} = -u_j^{(0)} \frac{du_j^{(0)}}{dz}\chi + \nu \frac{\partial^3 \psi}{\partial y^3} . \tag{S19}$$

The interface between spore laden and clean air can then be identified with the streamfunction $\psi = 0$, and the indicator function χ equal to 0 or 1 according as $\psi \gtrless 0$.

A method for solving boundary layer flows driven by spatially varying velocity fields was derived by Görtler [15], namely, we introduce similarity variables for the streamwise, and

width directions:

$$\xi = \frac{1}{\nu}\int_0^z u_j^{(0)}(z')\,\mathrm{d}z' \quad \text{and} \quad \eta = \frac{u_j^{(0)}(z)y}{\sqrt{2\nu\xi}}\ , \tag{S20}$$

and posit that the stream function takes functional form:

$$\psi = \nu\sqrt{2\xi}F(\xi,\eta)\ , \tag{S21}$$

so that [15]:

$$\frac{u}{u_j^{(0)}} = \frac{\partial F}{\partial \eta} \quad \text{and} \quad \frac{v}{u_j^{(0)}} = -\frac{1}{\sqrt{2\xi}}\left(F + 2\xi\frac{\partial F}{\partial \xi} + (\beta(\xi)-1)\,\eta\frac{\partial F}{\partial \eta}\right)\ . \tag{S22}$$

where the function $\beta(\xi)$ is a dimensionless measure of the rate of deceleration of the surrounding fluid:

$$\beta(\xi) \equiv \frac{2\nu u_j^{(0)\prime}(z)\xi}{u_j(z)^{(0)^2}}\ . \tag{S23}$$

The boundary layer equation (S19) can then be written in the form:

$$\frac{\partial^3 F}{\partial \eta^3} + F\frac{\partial^2 F}{\partial \eta^2} + \beta(\xi)\left(\chi(F) - \left(\frac{\partial F}{\partial \eta}\right)^2\right) = 2\xi\left(\frac{\partial F}{\partial \eta}\frac{\partial^2 F}{\partial \eta \partial \xi} - \frac{\partial F}{\partial \xi}\frac{\partial^2 F}{\partial \eta^2}\right)\ , \tag{S24}$$

The boundary layer velocity must match on one side to the jet, and on the other side to the quiescent fluid surrounding the jet, imposing boundary conditions $\frac{\partial F}{\partial \eta} \to 1$ or 0 as $\eta \to \mp\infty$. For the third boundary condition we use Ting's result that the boundary layer neither gains nor loses momentum to the surrounding flows by advection [12], which in this case implies that $v \sim -y u_j^{(0)\prime}(z)$ as $\eta \to -\infty$ or $F \sim \eta + o(1)$. The outer velocity enters into this boundary layer equation in just two places: directly, through the construction of $\beta(\eta)$, and indirectly through the shifting of the dividing stream line $F = 0$ away from $\eta = 0$, in the parameter χ.

We follow Görtler's approach of solving this equation for arbitrary jet speeds $u_j^{(0)}$, by series expansion in the variable ξ: $F(\eta) = F_0(\eta) + O(\xi)$. In order to obtain a closed form analytic expression for the drag on the jet, it is necessary to simplify the second, indirect dependence of Eq.(S24) upon the velocity of the jet. We take $\chi(F) \approx \chi(F_0)$: physically this means that we do not consider the effect of the deceleration of the jet when we determine its width [defined as the displacement of the streamline that divides spore laden from clean air], although we do consider the stronger effect of viscous spreading. This makes intuitive sense, because spores will tend to keep to their original trajectories and thereby move across

streamlines if subject to any shear on a time scale less than their response time scale (see Section I). We also checked the validity of the approximation by solving the perturbation series using the unapproximated density function $\chi(F)$, for a single specific jet velocity $u_j^{(0)}(z)$: in this case the difference between approximately and exactly computed $u_j^{(1)}(z)$ profiles was negligible.

We expand both the jet speed $u_j^{(0)}$ and deceleration β as power series in ξ: $u_j^{(0)} = \sum_n U_n \xi^n$ and $\beta = \sum_n b_n \xi^n$. We obtain the power series expansion for $u_j^{(0)}$ from the force balance Eq.(1), which can be recast in terms of the variable ξ as:

$$(\rho + \rho_s)\, {u_j^{(0)}}^2 \frac{du_j^{(0)}}{d\xi} = -\rho_s \nu g \ , \tag{S25}$$

and then compute the coeffs b_i by inputting this expansion into Eq.(S23). We find that the first four terms of each series suffice to completely capture the profile of the jet, and give the corresponding coefficients in Table S3.

b_0	0	U_0	U
b_1	$\frac{2U_1}{U_0}$	U_1	$-\frac{2\rho V^3}{3(\rho+\rho_s)U_0^2}$
b_2	$\frac{2(2U_0U_2-U_1^2)}{U_0^2}$	U_2	$-\frac{U_1^2}{U_0}$
b_3	$\frac{2(U_1^3-3U_0U_1U_2+3U_0^2U_3)}{U_0^3}$	U_3	$-\frac{U_1^3+6U_0U_1U2}{3U_0^2}$

Table S3: Coefficients for the series expansions of the acceleration $\beta(\xi)$ and velocity $u_j^{(0)}$. We define two constant velocities: U, the previously defined velocity of the jet at the start of the deceleration region, and a gravitational speed $V \equiv (g\nu)^{1/3}$.

The corresponding expansion for the boundary layer streamfunction has a form:

$$\begin{aligned} F(\xi,\eta) \ = \ & f_0(\eta) + b_1\xi f_1(\eta) + \xi^2\left(b_2 f_2(\xi) + b_{11}^2 f_{11}(\xi)\right) \\ & + \xi^3\left(b_3 f_3(\eta) + b_1 b_2 f_{12}(\eta) + b_1^3 f_{111}(\eta)\right) + O(\xi^4) \ , \end{aligned} \tag{S26}$$

where the functions $f_i(\xi)$ satisfy ordinary differential equations very similar to those presented by Görtler [15], with boundary conditions $f_0 \sim \eta + o(1)$ (& $f_i \to 0$ for all $i \neq 0$) as $\eta \to -\infty$ and $f_i' \to 0$, for all i, as $\eta \to \infty$. We solve these equations using numerical shooting on the unknown values of $f_i(0)$, $f_i'(0)$, $f_i''(0)$ [16]. The viscous stress upon the spore jet is then given by:

$$\eta \left.\frac{\partial u}{\partial y}\right|_{\psi=0} = \frac{\rho {u_j^{(0)}}^2}{\sqrt{2\xi}} \left.\frac{\partial^2 F}{\partial \eta^2}\right|_{F=0} \approx \frac{\rho {u_j^{(0)}}^2}{\sqrt{2\xi}} \left.\frac{\partial^2 F}{\partial \eta^2}\right|_{\eta=\eta_0} \tag{S27}$$

$f_0''(\eta_0)$	-0.2824
$f_1''(\eta_0)$	-0.2523
$f_2''(\eta_0)$	-0.2111
$f_{11}''(\eta_0)$	0.0408
$f_3''(\eta_0)$	-0.1863
$f_{12}''(\eta_0)$	0.0572
$f_{111}''(\eta_0)$	-0.0074

Table S4: Contributions at each order of ξ to the total viscous stress on the dividing streamline $f_0 = 0$.

where we define $\eta_0 = 0.374$ as the leading order dividing streamline between spore laden and clean air $F_0(\eta_0) = 0$. The boundary layer stress can therefore be simply evaluated once given the coefficients b_n from Table S3 and all of the second derivatives $f_i''(\eta_0)$, which we tabulate for the reader in Table S4.

To obtain the viscous correction to the total flow field, we substitute for $F_b[u_j^{(0)}] = \frac{2\eta}{a}\frac{\partial u}{\partial y}\Big|_{\psi=0}$ in Eq.(S15). If we rewrite this equation in terms of the variable ξ, then a few simple arrangements bring the equation into a particularly simple form:

$$\frac{d}{d\xi}\left((\rho+\rho_s){u_j^{(0)}}^2 u_j^{(1)}\right) = \frac{\nu}{A_j^{(0)}} F_b[u_j^{(0)}] \; . \tag{S28}$$

We can then solve for $u_j^{(1)}$ by integrating Eq.(S28) analytically in ξ.

The expression for the range arrived at by setting $u_j^{(0)} + u_j^{(1)} = 0$ predicts very well the range of the jet, for instance for the apothecium of diameter 2 mm shown in the main body of the paper we predict the length of the decelerating region $(z_{\max} - z_I)$ to be 73 mm, which is very close to the actual value of 70 mm. However, it can not capture the profile both near $z = z_{\max}$ and at $z = z_I$, and so the agreement in respect of range arises in some part, from serendipitous cancellation of errors of opposite sign. We make two modifications to the perturbation expansion in order to bring the predicted profile into exact agreement with the results of our DNS:

(i) It is not correct to identify $z = z_I$ as the onset of the viscous boundary layer. In fact we expect the boundary layer to start developing from $z = 0$, where the air is first set into motion (Fig S7). By the time that the jet starts to decelerate, this boundary layer has

reached a thickness $\delta_I \approx (\nu \int_0^{z_I} u_j^{(0)}\,\mathrm{d}z)^{1/2}/u_j^{(0)}$, where $u_j^{(0)}$ is given by the expression (in Section IV A). We model the finite initial thickness of the viscous boundary layer by introducing a virtual origin at a height $z = z_v$, chosen so that over the distance $z_v < z < z_I$, the jet boundary layer has developed to the required distance δ_I. In general it sufficed to take $z_I - z_v \lesssim 3$ mm

(ii) Because of the densification of a decelerating jet, gravitational forces always dominate over viscous stresses near $z = z_{\max}$. Mathematically, the final stages deceleration are governed by a dominant balance between the second term on the left hand side of Eq.(1) and the first term on the right hand side, leading a jet profile that is almost parabolic ${u_j}_s^2 \sim \frac{2\rho_s g(z_{\max}-z)}{\rho+\rho_s}$. This behavior is not reproduced by our two term solution, but we would expect it to be reproduced if sufficiently many terms of the perturbation series $u_j = u_j^{(0)} + u_j^{(1)} + \ldots$ were computed. To capture the final stages of deceleration without additional computation, we match directly the known singular behavior of the jet ${u_j}_s$ onto our first order approximant $u_j^* = u_j^{(0)} + u_j^{(1)}$. We choose matching point, which we denote by $z = z_m$, by first calculating the velocity gradient $u_j^{*\prime} = du_j^*/dz$ where $u_j^* = 0$ and then taking z_m to satisfy matching criteria $d{u_j}_s/dz = u_j^{*\prime}$ and ${u_j}_s = u_j^*$.

For apothecia that are large enough that the spore jet reaches a steady state before the end of the puff, these asymptotic approximations give excellent agreement with our DNS (Fig. 1D, 2A), and confirm that jet range can be determined simply by consideration of the weight of the spores, and boundary layer drag.

V. DYNAMICS OF THE LAYER OF AIR ENTRAINED BY A SHEET OF UPWARD MOVING SPORES

In the main text (Materials and Methods), we derived relations for the dependence of jet speed, u_j and thickness, δ_j, upon height above the originating fruit body:

$$u_j \sim \left(\frac{\zeta^2 Q_s^2 \nu z}{\mu^2}\right)^{1/3} \quad \text{and} \quad \delta_j \sim \left(\frac{\mu\nu z}{\zeta Q_s}\right)^{1/3} \tag{S29}$$

These scalings are well supported by our DNS (Fig S8).

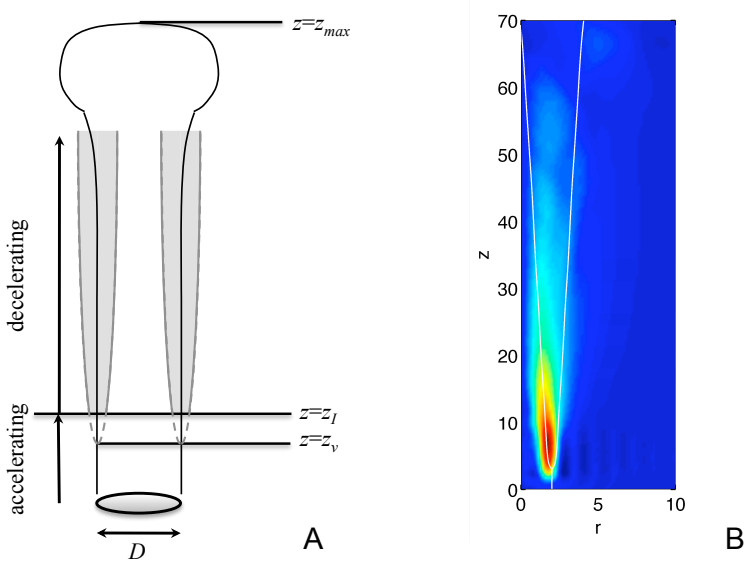

Figure S7: (A) Schematic showing the two regions of the spore jet, and the boundary layer of highly sheared air surrounding the central jet. (B) Color plot of the velocity gradients within the jet shows that gradients are sharply peaked at the jet boundary, a region that grows in accordance with boundary layer scalings (white curves). Note the different scalings of the vertical (z) and horizontal (r) axes.

VI. STATISTICS OF SPORE EJECTION TIMES IN *ASCOBOLUS* CF. *FURFURACEUS*

Here we present spore ejection time data for two different *A.* cf. *furfuraceus* apothecia representing extremes in spore density and fruit body size from ten synchronous spore ejections captured using high speed imaging (see Sec. II). We measured the time lag between arrival of the triggering signal and the actual instant of spore ejection for every ascus. The resulting distribution shows that spores do not precisely eject upon arrival of the triggering signal but lag or lead it by tens of milliseconds. Remarkably the distribution of these time lags are identical, despite differences in size of the apothecia and number of spores (Fig. S9). In particular the similarity in the variances of the two distributions suggests that the individual time lags do not result from random noise which would yield a variance proportional to the total number of spores. Moreover the measured dispersion in ejection times closely matches our predictions for the thickness of the air layer entrained by the spores [18], consistent with

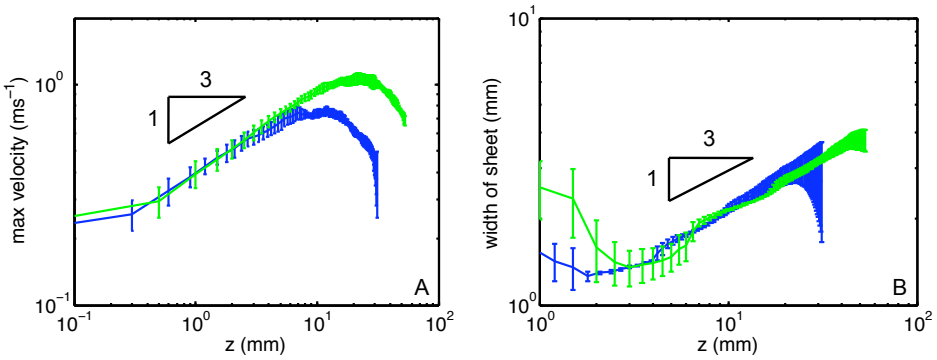

Figure S8: The velocity and thickness of the air layer entrained by sheet of spores agree with the scalings established in the main text. (A) Time averaged maximum upward velocity of air in the sheet is plotted against height above the apothecium. We measure the velocity of air along a line equidistant from the edges of the sheet. (B) Time averaged thickness of the sheet plotted against height above the apothecium. The sheet thickness is defined as the distance over which the air velocity decreases from u_j to $0.1 \times u_j$ (and, because of the blunting of the simulated velocity profile we use the predicted value of u_j, rather than the simulated center-line velocity, when determining jet width). In both panels the black triangle shows the predicted scaling, from boundary layer theory, and blue data correspond to $v_s = 2\,\mathrm{m{\cdot}s^{-1}}$, and green data to $v_s = 4\,\mathrm{m{\cdot}s^{-1}}$.

selection upon ejection times due to hydrodynamic policing against cheating.

---

[1] Crowe C, Troutt R, Chung JN (1996) Numerical models for two-phase turbulent flows. *Annu Rev Fluid Mech* 28:11–43.

[2] Sundaram S, Collins LR (1999) A numerical study of the modulation of isotropic turbulence by suspended particles. *J Fluid Mech* 379:105–143.

[3] Buller AHR (1958) *Researches on Fungi, Vol. VI* (Hafner, New York, N.Y.).

[4] Quartapelle L (1993) *Numerical solution of the incompressible Navier-Stokes equations* (Birkhauser, Basel).

[5] Sundaram S, Collins LR (1996) Numerical considerations in simulating a turbulent suspension of finite-volume particles. *J Comput Phys* 124:337–350.

[6] Elghobashi S, Truesdell JC (1993) On the two-way interaction between homogeneous turbu-

lence and dispersed solid particles. ii: Turbulence modification. *Phys Fluids A* 5:1790–1801.

[7] Kohn L (1979) A monographic revision of the genus sclerotinia. *Mycotaxon* 9:365–444.

[8] Yafetto L, *et al.* (2008) The fastest flights in nature: high-speed spore discharge mechanisms among fungi. *PLoS One* 3.

[9] Roper M, Pepper RE, Brenner MP, Pringle A (2008) Explosively launched spores of ascomycete fungi have drag minimizing shapes. *Proc Nat Acad Sci USA* 105:20583–20588.

[10] White FM (2005) *Viscous fluid flow* (McGraw-Hill, New York, USA), 3rd edn.

[11] Pruppacher HR, Steinberger EH (1968) An experimental determination of the drag on a sphere at low Reynolds numbers. *J Appl Phys* 39:4129–4132.

[12] Schlichting H, Gersten K (2000) *Boundary-layer theory* (Springer, Berlin, Germany), 8th edn.

[13] Turner JS (1980) *Buoyancy effects in fluids* (Cambridge University Press, Cambridge, U.K.).

[14] Batchelor G (1967) *Introduction to Fluid Dynamics* (Cambridge University Press, Cambridge, U.K.).

[15] Görtler H (1957) A new series for the calculation of steady laminar boundary layer flows. *J Math Mech* 6:1–66.

[16] Press W, Teukolsky S, Vetterling W, Flannery B (2007) *Numerical Recipes: The Art of Scientific Computing* (Cambridge Univ. Press, Cambridge, U.K.), 3rd edn.

[17] At moderate Reynolds numbers, the amount of fluid directly entrained by the spore scales with the spore size $\sim r^3$, so that by neglecting unsteady contributions we incur an error of order $O(\rho_s/\rho = 0.001)$. As the spore decelerates, the region of entrained fluid eventually grows like $\sim r/\mathcal{R}e$. In particular this suggests that the added mass of the fluid becomes comparable to spore inertia only when $\mathcal{R}e \approx (\rho/\rho_s)^{1/3} \approx 0.1$. However, at these Reynolds numbers viscous effects dominate over inertial effects, and the steady form of the Stokes drag law is certainly a good approximation.

[18] In fact because of the different spore densities we predict a slightly different thickness of the entrained air for the two apothecia. However, because $\delta_j \sim Q_s^{-1/3}$ the dependence of the thickness upon spore density is very weak.

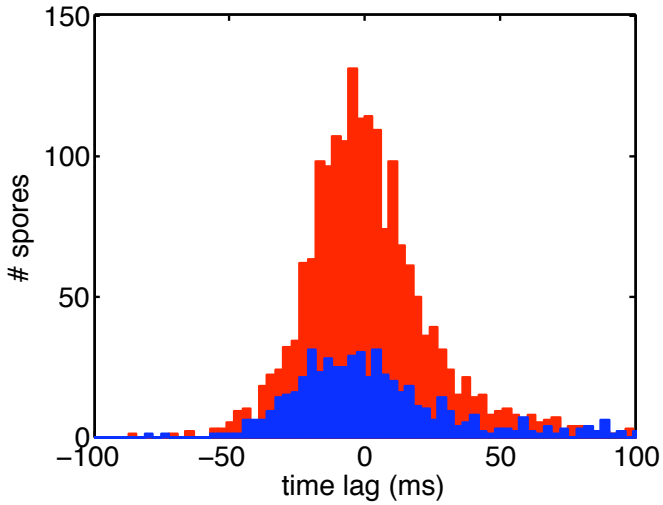

Figure S9: Histogram of spore ejection times measured from apothecia of *A.* cf. *furfuraceus* shows that spores do not eject precisely upon arrival of the wave of ejections. The two colors correspond to two apothecia: red, 14952 spores, diameter 1.5 mm, standard deviation 24 ms; blue, 4520 spores and diameter 4.0 mm, standard deviation 29 ms.